POAC'25
St. John's, Newfoundland and Labrador, Canada

Proceedings of the 28th International Conference on Port and Ocean Engineering under Arctic Conditions
Jul 13-17, 2025
St. John's, Newfoundland and Labrador
Canada

Trends in the Pack Ice Regime on Makkovik Bank, Offshore Labrador, 2003-2023

Ian D. Turnbull[1,2], Rocky S. Taylor[2], Tony King[1], Matthew Asplin[3,4], James Bartlett[3], Dawn Sadowy[3], Keath Borg[3], and Alka Dash[2]
[1] C-CORE, St. John's, Canada
[2] Memorial University of Newfoundland (MUN), St. John's, Canada
[3] ASL Environmental Sciences, Saanichton, Canada
[4] University of Victoria, Victoria, Canada

ABSTRACT

Climate change is causing significant changes in the global cryosphere, which will have wide-ranging impacts on weather, ocean conditions, marine and terrestrial life, ocean navigability, and offshore energy development. During 2003-2009, an Ice Profiling Sonar was deployed on the Makkovik Bank, offshore Labrador. The instrument collected draft data on pack ice that drifted overhead. In 2022, an Ice Profiling Sonar (IPS) was redeployed at approximately the same location as the 2003-2009 moorings. Changes in the pack ice regime on Makkovik Bank over the period 2003-2023 are examined and linked to the changing metocean environment in terms of the atmospheric and surface ocean temperatures and heat fluxes. A general warming trend in the atmospheric temperatures and a trend toward less severe pack ice conditions was observed over the 2003-2023 period. Potential future trends in the pack ice regime are also explored using climate model output to 2050. The IPS was redeployed for the 2023-2024 and 2024-2025 ice seasons with the intent to create a longer term-record of ice conditions to assess trends into the future.

KEY WORDS: Offshore Labrador; Pack ice; Ice thickness; Ice measurement; Climate change.

INTRODUCTION

The global cryosphere is undergoing significant changes due to climate change. The cryosphere is tightly coupled to atmospheric and oceanic conditions such as temperatures, current patterns, and salinity. Changes in the cryosphere are therefore likely to cause significant changes in global weather patterns, ocean conditions, and marine and terrestrial life. These changes will additionally affect humans through changes in ocean navigability, fisheries, and offshore energy development. Offshore Newfoundland and Labrador (NL) in eastern Canada is one of the southernmost regions of the global cryosphere and is experiencing increasingly unpredictable interannual variations in seasonal ice severity as climate change continues (e.g., see Han, et al., 2019). For example, King and Turnbull (2022) and King, et al. (2023) documented a reduction in the seasonal numbers and sizes of icebergs offshore southeastern Newfoundland over the last few decades coinciding with warming air and ocean temperatures. Han et al. (2019) shows reductions in the projected probability of pack ice presence along the

NL coast in terms of extent and concentration out to 2069. During the 1991-2020 period, the seasonal number of days with open water has increased along the NL coast (e.g., see Oilco, 2022). This paper focuses on trends in pack (sea) ice conditions in the offshore region of central Labrador known as the Makkovik Bank.

During 2003-2009, an Upward-Looking Sonar (ULS)/Ice Profiling Sonar (IPS) was deployed on the Makkovik Bank (see Figure 1), by Fisheries and Oceans Canada (DFO), with ASL Environmental Sciences performing the data analysis (ASL Environmental Sciences Inc., 2009). The instrument collected draft data on pack ice, as well as a limited number of icebergs that drifted overhead. In 2022, efforts to collect ice draft data on Makkovik Bank were renewed by C-CORE, ASL, and Memorial University of Newfoundland (MUN), and an IPS was redeployed at approximately the same location as the 2003-2009 moorings. Data collection on the Makkovik Bank remains ongoing at the time of writing this paper. This paper examines trends in the pack ice regime on Makkovik Bank over the period 2003-2023 and links them to changes in the metocean environment in terms of the atmospheric and surface ocean heat fluxes. Potential future trends in the pack ice regime are also explored using climate model output to 2050.

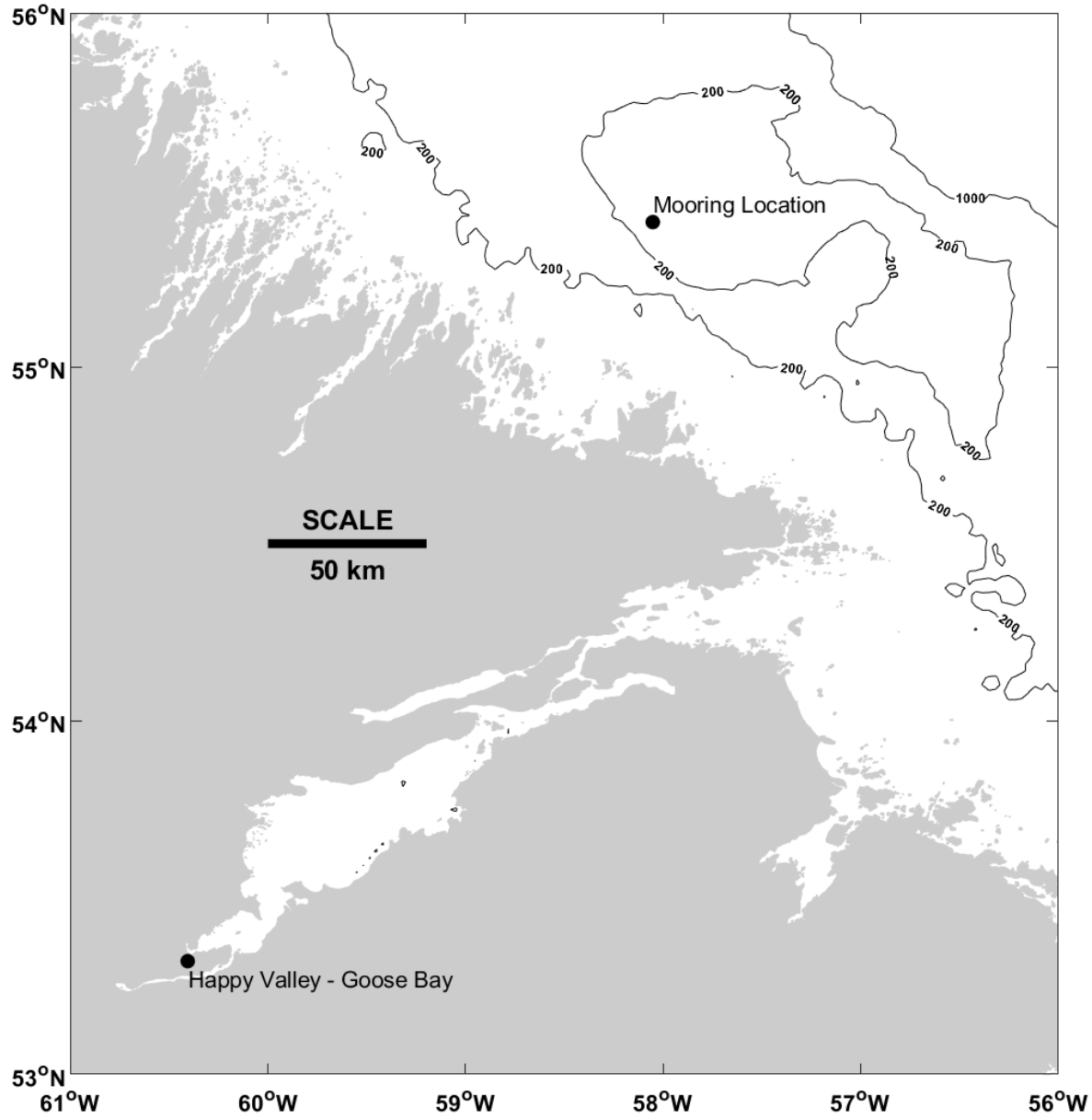

Figure 1. Deployment location for the Makkovik Bank mooring.

MOORING DEPLOYMENTS AND DATA COLLECTION

The IPS is manufactured by ASL and records ice draft (keel depth) data by determining the return travel time of an acoustic pulse (420 kHz; 1.8° beam at 3 dB) reflected off the underside of the ice and multiplying by the speed of sound in seawater (see Figure 2 and ASL Environmental Sciences Inc., 2024). The instrument integrates a Paroscientific Digiquartz® pressure sensor, offering a depth measurement accuracy of 0.01% of full scale (0-126 m range), with a fine resolution of 0.003 m. Additionally, the IPS includes a precision tilt sensor with an accuracy of ±0.5° and a resolution of 0.01°, allowing for accurate correction of instrument orientation. A temperature sensor with an accuracy of ±0.1°C and resolution of 0.05°C further enhances environmental data quality with an ice draft accuracy of ±0.05 m, assuming proper correction for sound speed and water density variations, with a resolution of 0.01 m. The IPS

unit was deployed at 96 m depth for the 2022-2023 ice season (and similar water depths for the pre-2010 deployments).

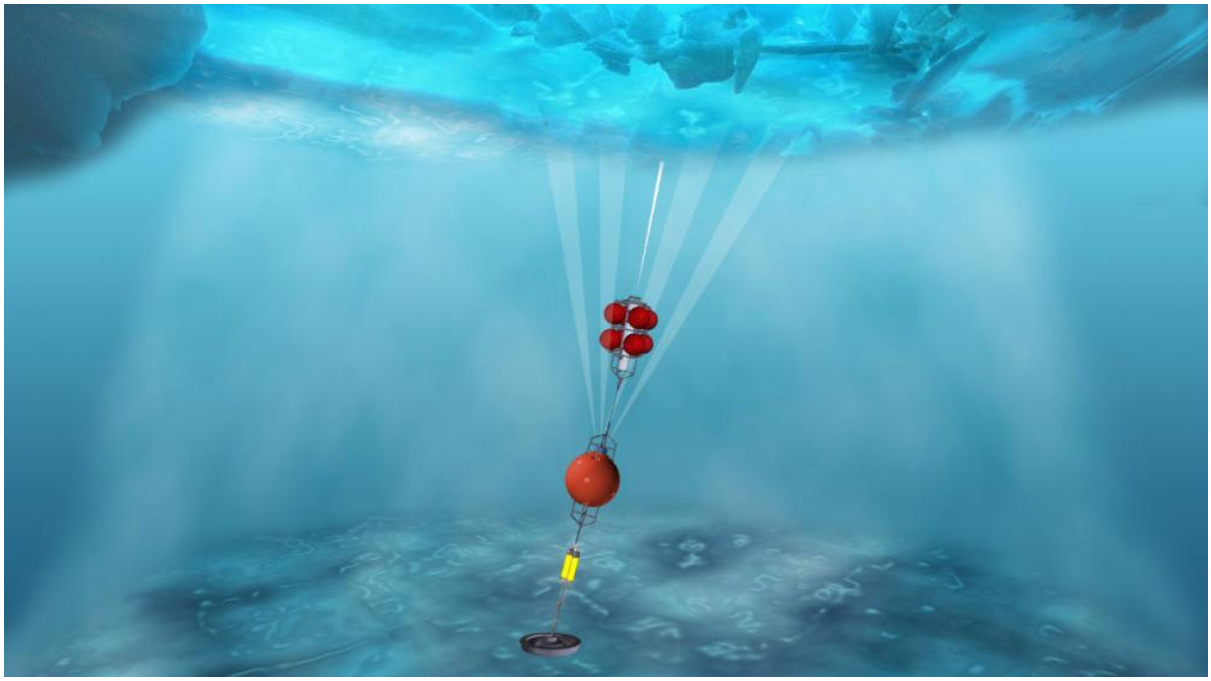

Figure 2. Upward-looking IPS mooring (image courtesy of ASL).

Table 1 shows the locations and ice season periods for each of the IPS deployments over 2003-2023. The IPS was typically deployed in November of the prior year before the start of freeze-up. In the present analysis, the ice season period was considered as the first to the last day of appearance of ice at least 5 cm thick.

Table 1. Makkovik Bank mooring deployment locations and ice season periods.

Year	Location	Period	Days
2003	55.409983°N/58.0634°W	January 12 – June 1	141
2005	55.4094°N/58.0636°W	January 4 – May 11	127
2007	55.4079°N/58.0632°W	January 2 – June 29	178
2009	55.412°N/58.0652°W	January 11 – June 18	158
2023	55.4088°N/58.0518°W	January 26 – June 26	151

Figure 3 shows an example of pack ice draft data collected over March 15, 2023. Icebergs were filtered out of the datasets by manual interpretation as icebergs typically have very steep keel walls and relatively deep drafts compared to the ice immediately on either side.

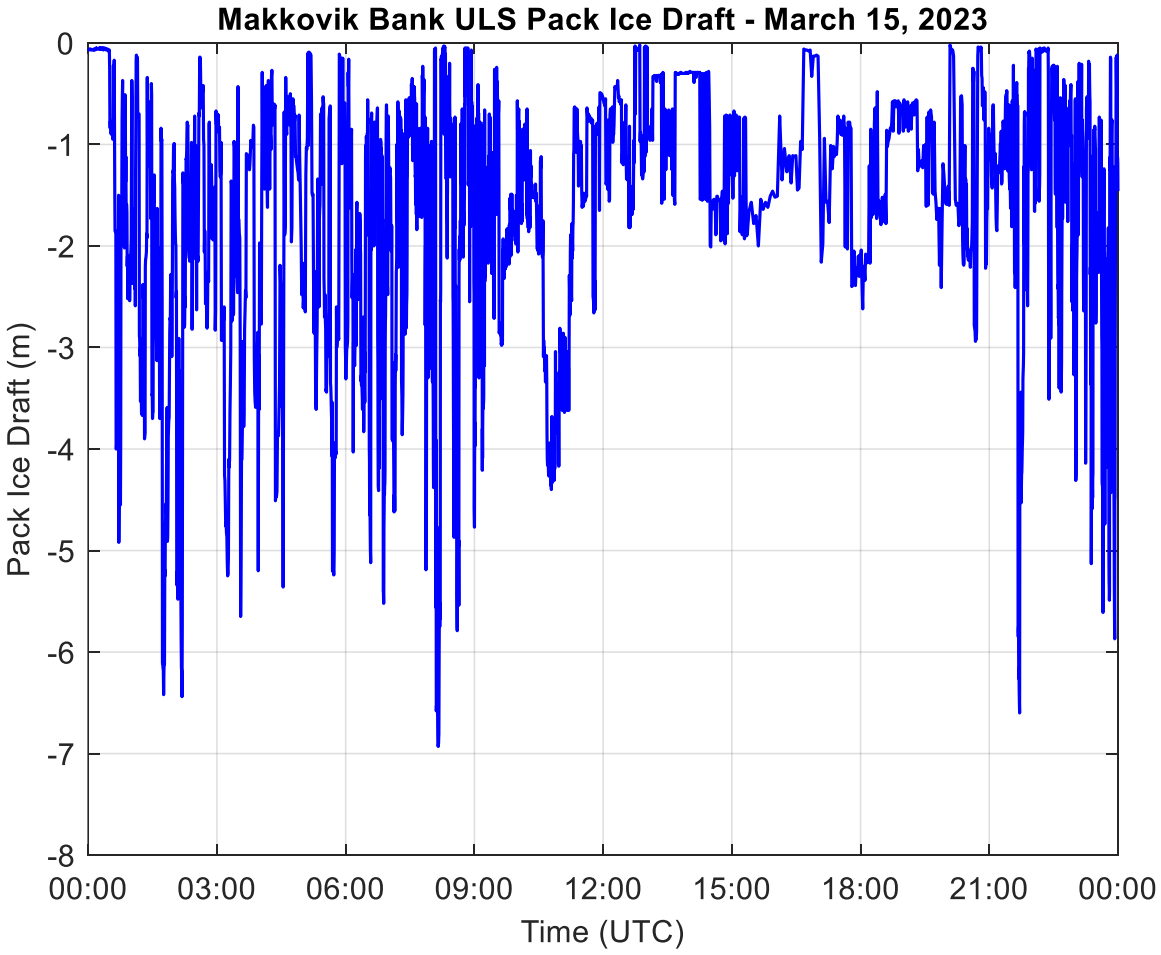

Figure 3. Sample of ULS/IPS ice draft data.

PACK ICE THICKNESS AND SEASON LENGTH

The ice draft data were converted to thickness using the Archimedes principle (e.g., see Bourke and Paquette, 1989):

$$h_i = h_d \left(\frac{\rho_w}{\rho_i}\right), \quad (1)$$

where h_i is the ice thickness (meters), h_d is the ice draft (m), ρ_w is the density of seawater (1026.5 kgm^{-3}), and ρ_i is the density of sea ice (920 kgm^{-3}). Figure 4 shows the exceedance probabilities for pack ice thicknesses for each seasonal IPS deployment over 2003-2023. In terms of extreme pack ice features (e.g., ridge keels), the 2023 pack ice season was the second least severe after 2005, with the deepest keels observed in 2003, 2007, and 2009. While it is beyond the scope of this paper to analyze ridged versus level ice, the tails of the exceedance probability distributions in Figure 4 show extreme ridged ice thicknesses of 25-35 m in 2003, 2007, and 2009, while only reaching 15-25 m in 2005 and 2023. Exceedance probabilities for ice thicknesses less than 5 m indicate the least severe seasons for level ice thickness were 2005 and 2023, which is corroborated with the seasonal mean ice thicknesses shown in Figure 6.

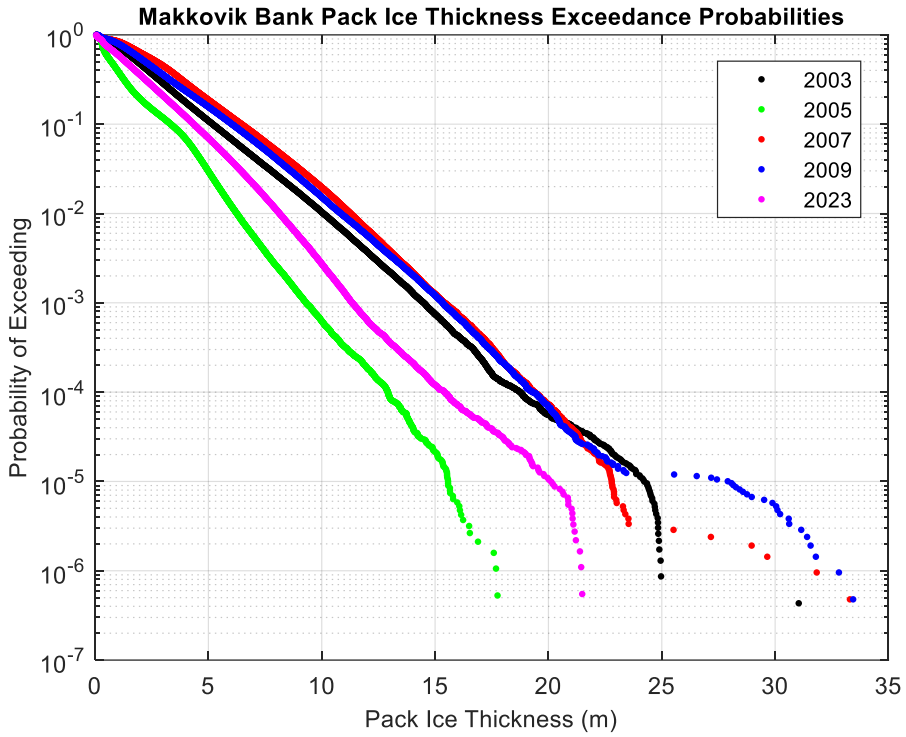

Figure 4. Pack ice thickness exceedance probabilities on Makkovik Bank.

Figure 5a shows the daily mean ice thickness for each season at the IPS deployment locations and Figure 5b shows the total ice season lengths (the blue line shows the linear trend based on least-squares regression and the red lines show the upper and lower bounds of the 95% confidence interval). The 2007 ice season was the longest of the five, and had the latest occurrence of daily mean ice thickness greater than 3 m. Although there is a slight trend toward longer ice seasons, this is based on very limited data (five seasons) thus far, and the 2023 season showed a significant decrease in daily mean ice thickness to below 3 m after only 80 days, from which it did not recover. The other four pre-2010 ice seasons all showed later significant decreases in daily mean ice thickness, with the 2003 and 2009 seasons showing some recovery above 3 m. Slopes and R^2 values for all least-squares linear regression lines shown in this paper are provided in Table 3.

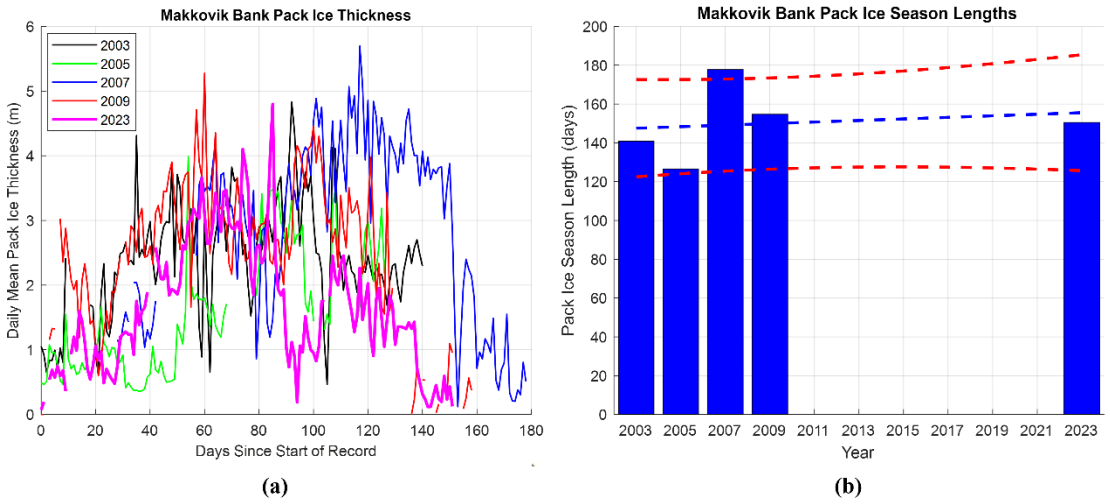

Figure 5. Makkovik Bank pack ice thickness since start of ice season (a) and ice season length (b).

Figure 6 shows the mean, maximum, and standard deviation (±1 standard deviation (σ) about the mean in Figure 6a) in pack ice thickness for each of the five ice seasons on the Makkovik Bank. From 2003-2023, a trend toward lower average (blue dotted least-squares linear regression line in Figure 6a) and maximum (red dotted least-squares linear regression line in Figure 6b) pack ice thicknesses and less variable thicknesses is apparent.

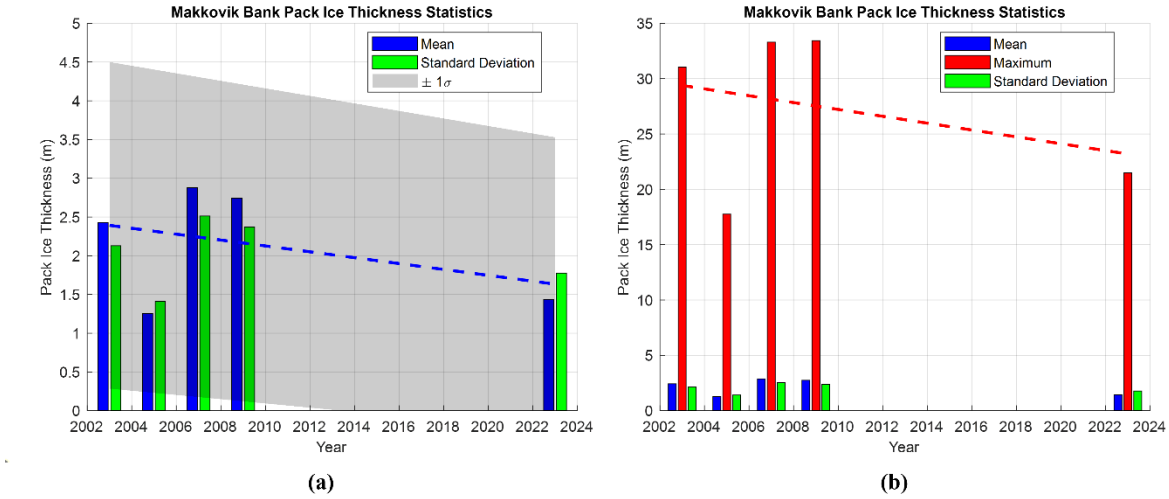

Figure 6. Makkovik Bank pack ice thickness seasonal statistics.

CLIMATOLOGY ANALYSIS

In this section, the climatology trends on the Makkovik Bank and the remaining offshore region of Labrador to the north over 2003-2023 are explored and linked to the trends in pack ice thickness presented in the previous section. It is informative to examine the climatology of the more northern region as this is the source region for the ice that drifts southward over the Makkovik Bank. The primary metocean variables that control seasonal ice growth and melt are the air temperature, sea surface temperature (SST), and the associated surface and basal energy fluxes. Regional pack ice concentration is also of interest as it provides an overall picture of seasonal ice conditions and severity, as well as seasonal Freezing Degree Days (FDDs) and

Melting Degree Days (MDDs). The FDD and MDD are direct functions of air temperature, providing a measure of the severity and duration of freezing or melting conditions, and are closely linked to the rates of thermodynamic ice growth and melt.

The hourly 2 m air and dew point temperature, SST, pack ice concentration, 10m wind velocity, total cloud area fraction, surface atmospheric pressure, and downward surface solar radiation were obtained for January-June for the five ice seasons over 2003-2023 from the ERA5 reanalysis (e.g., see Hersbach, et al., 2024). The atmospheric variables and SST were used to compute the energy fluxes that control the ice thermodynamics. The ERA5 reanalysis covers the globe at a 0.25° spatial resolution for 1940-present. Since it is not possible to examine regional climatological conditions for all five seasons for all metocean variables within the scope of this paper due to space limitations, regional examples for each variable are provided for 2003, the earliest season of data collection, and compared with 2023, the most recent season of data collection, to compare variables over the longest possible period. However, sea ice concentration for 2007 is compared with 2023 since the 2007 season had the highest mean sea ice concentration of all five seasons.

Air Temperature

Figure 7 shows the average January-June air temperature offshore Labrador from Makkovik Bank northward to 60°N for 2003 (a) and 2023 (b). The IPS mooring locations for both years are marked with a red dot. Warmer regional conditions in 2023 compared to 2003 are apparent as the coldest air in the northwest is about 1-2°C warmer in 2023. At the mooring location, 2023 was approximately 2°C warmer than 2003.

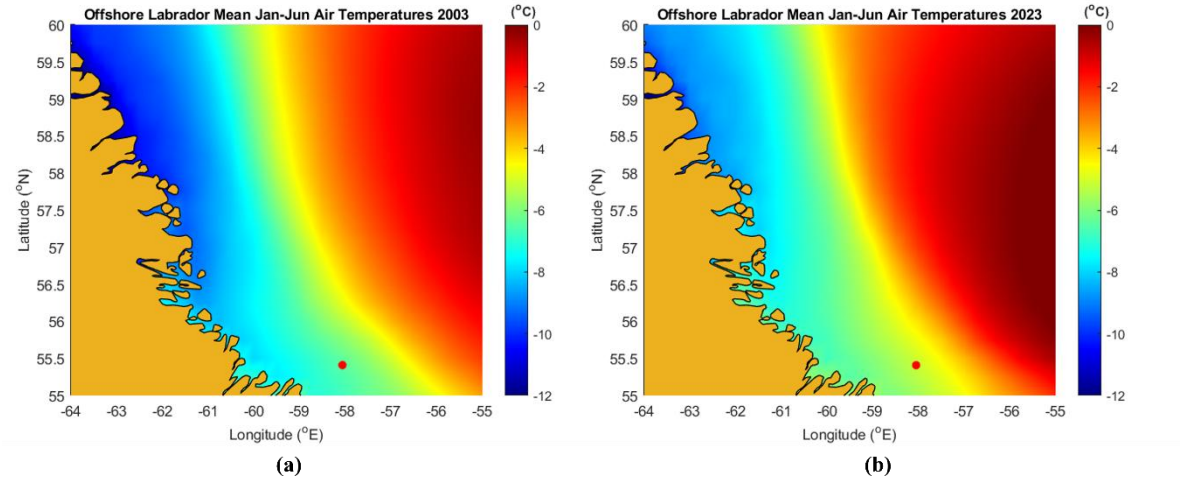

Figure 7. Offshore Labrador ice season mean air temperature in 2003 (a) and 2023 (b).

Sea Surface Temperature

Figure 8 shows the average January-June SST offshore Labrador from the Makkovik Bank northward to 60°N for 2003 (a) and 2023 (b). Regional mean SSTs were somewhat cooler in 2023 compared to 2003, despite the warmer air temperatures in 2023. This indicates that ocean current patterns in 2023 may have advected colder water into the region from further north and highlights the complexity of air and ocean temperature coupling. Colder water advection could have come from the increasing trend in Greenland glacier terminal melt. The colder SSTs in 2023 would have acted to preserve pack ice better than in 2003, in contrast with the warmer air temperatures in 2023 pointing toward increased ice melt and decreased ice growth.

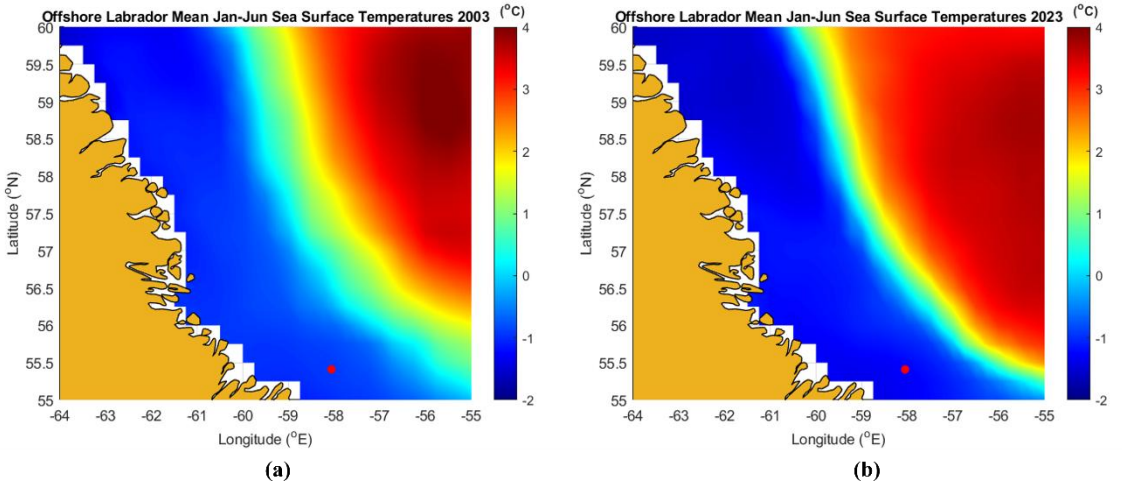

Figure 8. Offshore Labrador ice season mean SST in 2003 (a) and 2023 (b).

Ice Concentration

Figure 9 shows the average January-June pack ice concentrations offshore Labrador from the Makkovik Bank northward to 60°N for 2007 (a) and 2023 (b). The 2007 season was chosen as the pre-2010 year for this example since it featured the highest mean ice concentrations across the region of all five seasons. Average ice concentrations at the mooring location in 2007 were not significantly greater than in 2023 (around 6-7/10ths compared to 5-6/10ths in 2023), however, a band of 8/10ths+ average concentration ice existed along the coast in 2007 that was absent in 2023. Since ice observed at the mooring on the Makkovik Bank drifts in from the north, the higher regional concentrations of pack ice in 2007 likely contributed to the higher observed mean ice thicknesses when compared to 2023.

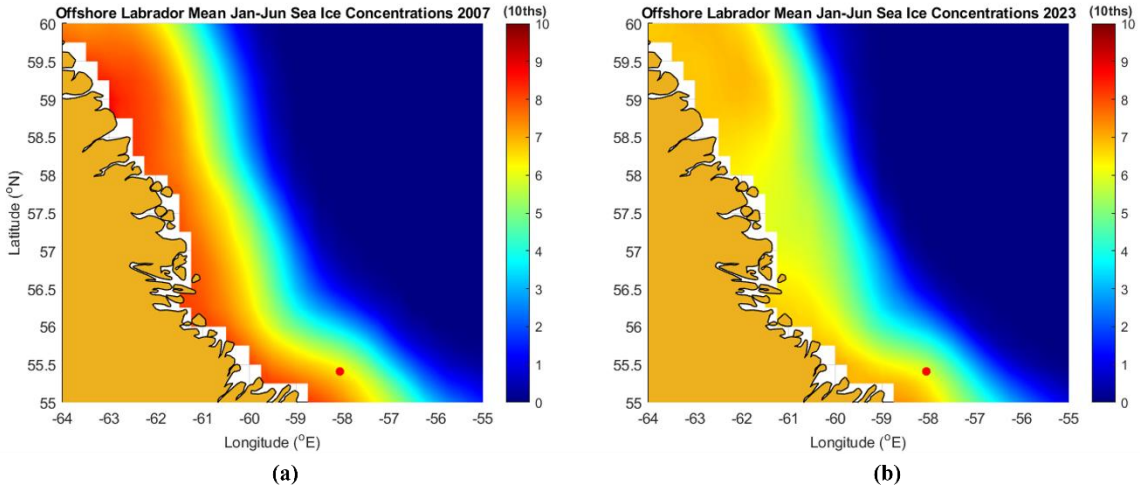

Figure 9. Offshore Labrador ice season mean sea ice concentration in 2007 (a) and 2023 (b).

Energy Fluxes

Changes in pack ice thickness are controlled primarily by the rates of energy input to the ice surface and base (thermodynamics), and by dynamic compression of pack ice under pressure from surrounding ice. This section examines the surface and basal energy fluxes into the ice pack during the five seasons of IPS deployments. Although ERA5 provides surface net energy

flux variables directly, they are assumed to be over open water. Therefore, in this paper, the energy fluxes over pack ice are calculated using the ERA5 air and dew point temperatures, SSTs, surface air pressures, cloud cover, wind speed, and downward solar radiation.

The net energy balance over the ice surface is the sum of the incoming and reflected solar radiation, incoming and outgoing longwave radiation, and the sensible and latent heat fluxes. The surface net solar radiation flux (F_{SW}, Wm^{-2}) is calculated according to (e.g., see Ebert and Curry, 1993):

$$F_{SW} = \big(1 - (0.18(1 - T_c) + 0.35T_c)\big)(1 - \alpha_i)S_R, \quad (2)$$

where T_c is the total cloud cover (area fraction), α_i is the ice albedo (assumed to be 0.6), and S_R is the downward solar radiation. The downward longwave radiation flux (F_{LW}, Wm^{-2}) is calculated according to:

$$F_{LW} = \epsilon_a \sigma T_a^4, \quad (3)$$

where ϵ_a is the atmospheric emissivity, σ is the Stefan-Boltzmann constant (5.669×10^{-8} $Wm^{-2}K^{-4}$), and T_a is the 2 m air temperature (K). The atmospheric emissivity is computed as (e.g., see Marks and Dozier, 1979, and Crawford, et al., 2015):

$$\epsilon_a = 1.24\left(\frac{e_a}{T_a}\right)^{\frac{1}{7}}, \quad (4)$$

where e_a is the atmospheric vapor pressure (hPa). The atmospheric vapor pressure is calculated as (e.g., see Murray, 1967, Ballicater Consulting Ltd., 2012, and Crawford, et al., 2015):

$$e_a = 6.108 \times \exp\left(\frac{17.296(T_a - 273.15)}{T_a - 35.86}\right)\left(\frac{RH}{100}\right), \quad (5)$$

where RH is the atmospheric relative humidity (%) which is calculated as a function of the air and dew point temperatures and saturation vapor pressure. The sensible heat flux (F_{sens}, Wm^{-2}) over pack ice is calculated according to (e.g., see Ebert and Curry, 1993):

$$F_{sens} = \rho_a c_{pa} C_T u_a (T_s - T_a), \quad (6)$$

where ρ_a is the air density (kgm^{-3}) calculated from the ideal gas law (it is approximately 1.225 kgm^{-3}), c_{pa} is the specific heat capacity of air at constant pressure (1005 $Jkg^{-1}K^{-1}$), C_T is a stability-dependent transfer coefficient, u_a is the wind speed (ms^{-1}), and T_s is the ice surface temperature (K). The ice surface temperature was assumed to be equivalent to the air temperature when it was below the freezing point of sea ice (-1.8°C or 271.35K) and was assumed to be -1.8°C when the air temperature was above this freezing point. The stability-dependent transfer coefficient is computed as (e.g., see Ebert and Curry, 1993):

$$C_T = C_{T0}\left(1 - \frac{2b'Ri}{1 + c|Ri|^{\frac{1}{2}}}\right), Ri < 0,$$

$$C_T = C_{T0}(1 + b'Ri)^{-2}, Ri \geq 0, \quad (7)$$

where C_{T0} is 1.3×10^{-3} over ice, b' is 20, c is $1961b'C_{T0}$ (50.986), and Ri is the bulk Richardson number. The Richardson number is calculated as (e.g., see Ebert and Curry, 1993):

$$Ri = \frac{g(T_a - T_s)\Delta z}{T_a u_a^2}, \quad (8)$$

where g is the Earth gravitational constant (9.80665 ms^{-2}) and Δz is the height of the winds (10 m). The latent heat flux (F_{lat}, Wm^{-2}) over pack ice is calculated according to (e.g., see Ebert and Curry, 1993):

$$F_{lat} = \rho_a L_v C_T u_a (q_{sat}(T_s) - q_a), \quad (9)$$

where L_v is the latent heat of vaporization of ice (2.501×10^6 Jkg^{-1}), $q_{sat}(T_s)$ is the saturation specific humidity at the ice surface temperature, and q_a is the atmospheric specific humidity. The specific humidities are calculated as functions of the ice surface, air, and dew point temperatures, and the surface atmospheric pressure. Finally, the net energy balance (F_{net}, Wm^{-2}) at the ice surface is (e.g., see Ebert and Curry, 1993):

$$F_{net} = \epsilon_i (F_{LW} - \sigma T_s^4) + F_{SW} - F_{sens} - F_{lat}, \quad (10)$$

where ϵ_i is the ice emittance (0.97).

Figure 10 shows the average January-June surface net energy balance over pack ice offshore Labrador from the Makkovik Bank northward to 60°N for 2003 (a) and 2023 (b). Note that while pack ice did not cover the entire region shown in Figure 10, the surface net energy flux was calculated assuming the presence of pack ice everywhere only for purposes of comparing the energy fluxes into the ice over each monitored ice season. The whole offshore Labrador region from the Makkovik Bank northward showed stronger surface net mean energy flux into the ice in 2023 compared to 2003, particularly at the mooring location. This would have contributed to increased ice melt and decreased ice growth over the season in 2023 compared to 2003.

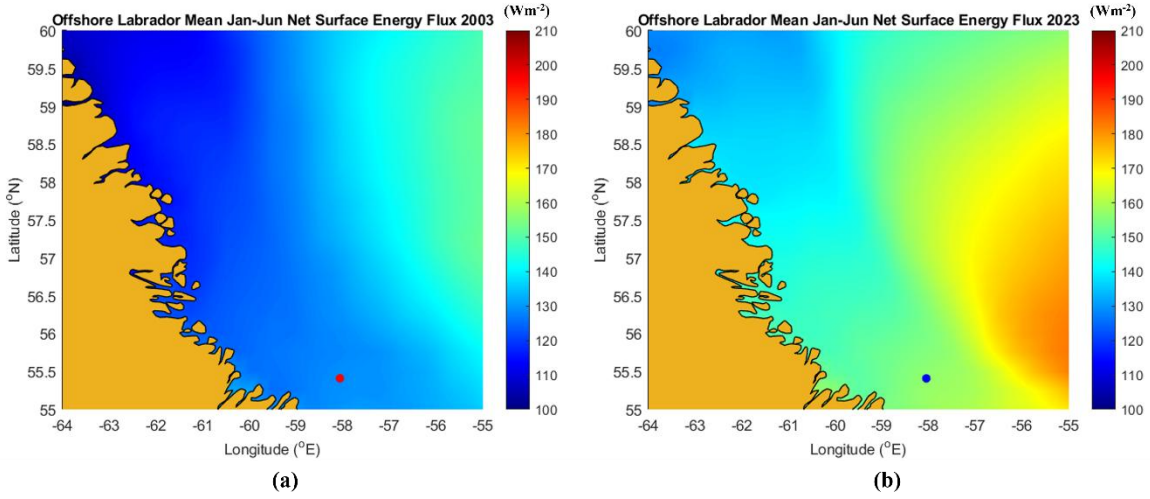

Figure 10. Offshore Labrador ice season mean net surface energy flux in 2003 (a) and 2023 (b).

Figure 11 shows the January-June mean net surface energy flux over pack ice at the mooring locations for each deployment season (a) and their January-June exceedance probabilities (b). There was a clear increasing trend in mean net surface energy flux into the pack ice over the five seasons (Figure 11a, the blue line shows the linear trend based on least-squares regression and the red lines show the upper and lower bounds of the 95% confidence interval), with the highest values for net surface energy flux having occurred in 2009 and 2023 (Figure 11b).

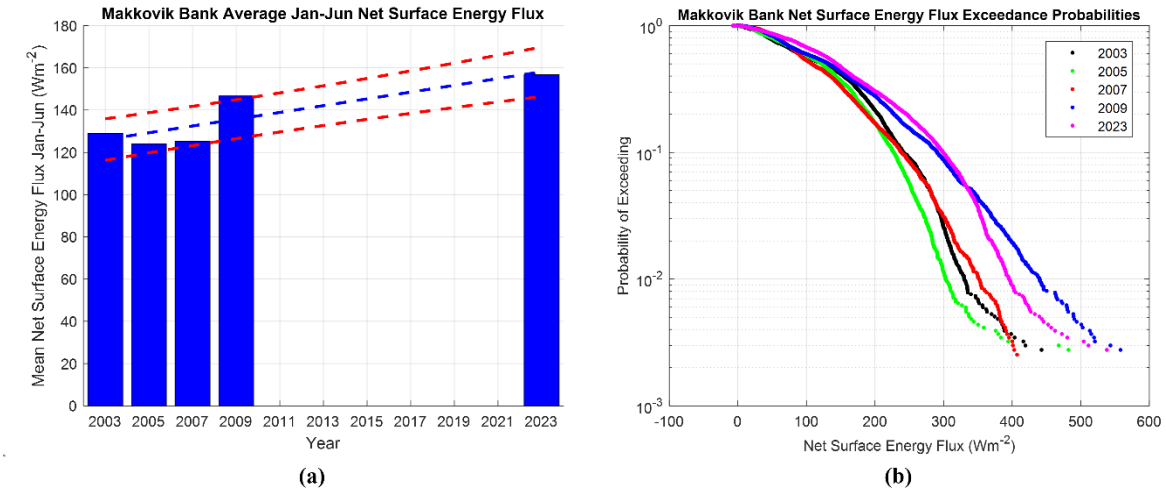

Figure 11. Makkovik Bank ice season net surface energy flux means (a) and exceedance probabilities (b).

Table 2 provides a breakdown of the January-June averaged (downward positive) components of the net surface energy fluxes over pack ice at the mooring locations for each IPS monitoring season. In Table 2 only the downward component of the longwave radiation is considered. No significant trend is apparent over the five seasons in the longwave radiation and the sensible and latent heat fluxes. However, there was a clear upward trend in the surface solar radiation, with the largest mean seasonal value occurring in 2023. This reflects a decreasing trend in cloud cover over the Makkovik Bank. It is therefore likely that the increase in solar radiation played a role in the decreasing trend in ice thickness over the five IPS deployment seasons through increasing surface melt of the ice.

Table 2. Mean January-June surface energy fluxes on the Makkovik Bank (Wm^{-2}).

Year	Solar Radiation	Longwave Radiation	Sensible Heat Flux	Latent Heat Flux
2003	41.3	369.9	-5.5	3.1
2005	22.3	384.4	-7.6	1.4
2007	33.3	381.9	-5.9	4.2
2009	58.0	374.5	-5.4	3.6
2023	62.3	382.7	-5.0	2.5

The energy flux at the base of the ice (Wm^{-2}) with leads is formulated according to (e.g., see Ebert and Curry, 1993):

$$F_b = \rho c_{pw} C_{Tb} (T_{wi} - T_b), \tag{11}$$

where ρc_{pw} is the volumetric heat capacity of seawater at constant pressure (4.19×10^6 $Jm^{-3}K^{-1}$), C_{Tb} is a bulk transfer coefficient, T_{wi} is the temperature of the mixed layer below the ice (SST in °C), and T_b is the basal temperature of the ice, fixed at -1.8°C (the sea ice freezing temperature). The bulk transfer coefficient is computed as a function of the ice thickness according to (e.g., see Ebert and Curry, 1993):

$$C_{Tb} = 1.26 \times 10^{-4} h_i^{-\frac{1}{2}}, h_i < 3\ m,$$
$$C_{Tb} = 7.27 \times 10^{-5}, h_i \geq 3\ m. \tag{12}$$

A constant ice thickness of 1 m was used for calculation of C_{Tb}, leading to $C_{Tb} = 1.26 \times 10^{-4}$.

Figure 12 shows the January-June mean ice basal energy flux at the mooring locations for each deployment season (a, the blue line shows the linear trend based on least-squares regression and the red lines show the upper and lower bounds of the 95% confidence interval) and their January-June exceedance probabilities (b). There was a decreasing trend in mean basal energy flux into the pack ice over the five seasons (Figure 12a), which would have counteracted the effects of the overall increase in net surface energy flux in terms of ice growth versus melt rates. This trend is consistent with the decrease in SSTs observed between 2003 and 2023 (see Figure 8). The highest values for basal energy flux occurred in 2009 (Figure 12b). The highest seasonal average value for basal energy flux occurred in 2005, coinciding with the lowest mean and maximum seasonal ice thickness (Figure 6).

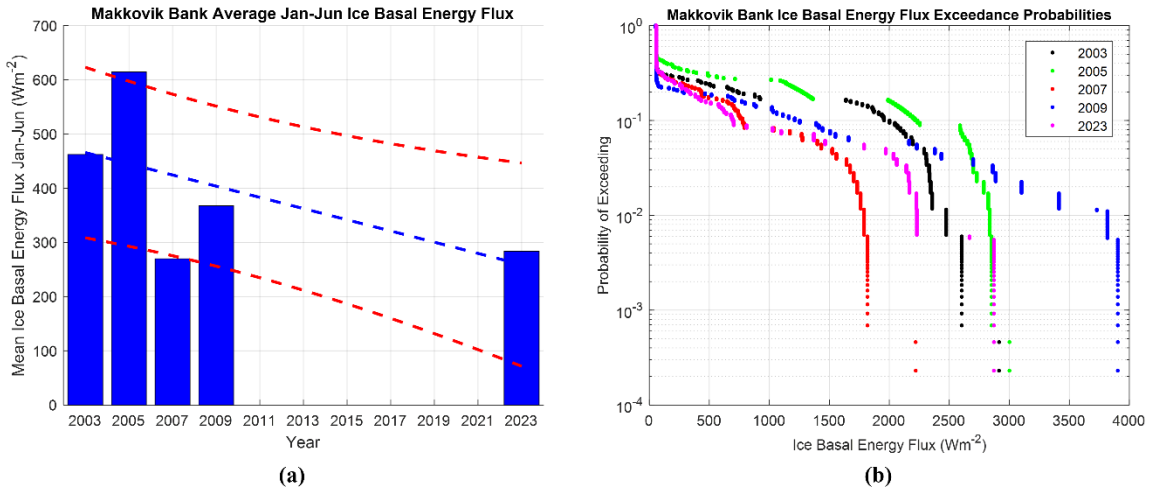

Figure 12. Makkovik Bank ice season basal energy flux means (a) and exceedance probabilities (b).

Freezing and Melting Degree Days

The January-June cumulative FDD and MDD were calculated for the IPS deployment seasons over the Makkovik Bank and northward offshore Labrador region to 60°N. The FDD and MDD are calculated as the cumulative sum of the differences between the daily mean air temperature and the seawater freezing temperature ($T_f = -1.8°C$) according to:

$$FDD\ or\ MDD = \sum_{i=1}^{N} T_a - T_f, \quad (13)$$

where $N = 181$ is the number of days in the January-June period. When the air temperature is above or below the freezing point, the daily FDD or MDD is zero, respectively. The cumulative FDD and MDD are a useful proxy for examining thermodynamic ice growth and melt rates over the course of an ice season.

Figure 13 shows the total January-June FDDs (note the color inversion whereby lower FDD totals are redder to denote warmer conditions) offshore Labrador from the Makkovik Bank northward to 60°N for 2003 (a) and 2023 (b). Warmer overall regional conditions are apparent in 2023 compared to 2003. This would have led to less ice growth in 2023, particularly in the northern source regions for the ice observed over the Makkovik Bank.

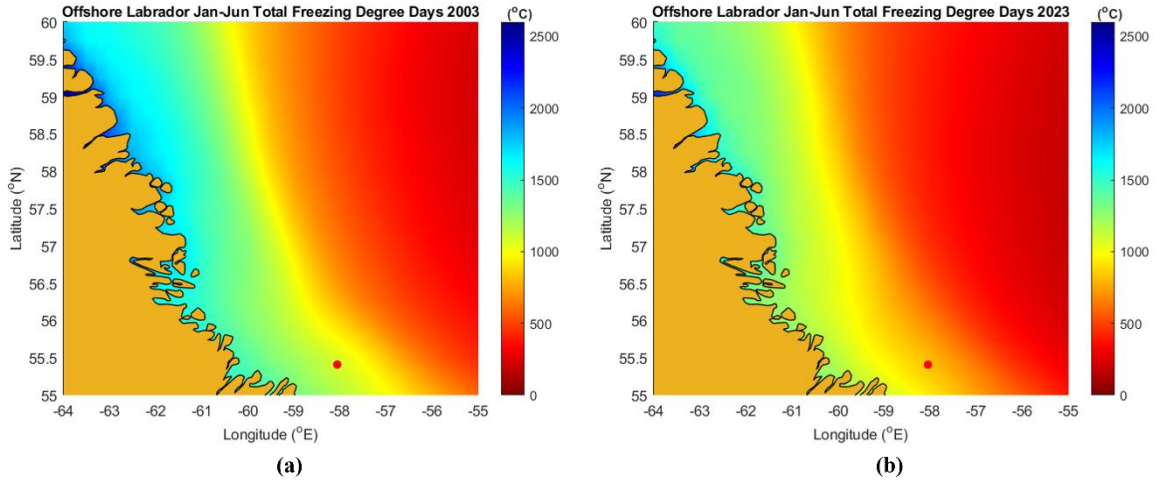

Figure 13. Offshore Labrador ice season cumulative FDDs in 2003 (a) and 2023 (b).

FUTURE CLIMATE CHANGE

Global climate change is expected to continue decades into the future as anthropogenic carbon emissions continue. Future climate change in particular regions is typically analyzed using global climate model projections, considering a range of potential future global carbon emissions scenarios. It is beyond the scope of this paper to consider all potential carbon emissions scenarios or output from all available climate models. Hence, output for the Makkovik Bank mooring location was obtained for one climate model from the latest Coupled Model Intercomparison Project Phase 6 (CMIP6) and for one future potential carbon emissions scenario.

The Australian Community Climate and Earth System Simulator (ACCESS) global climate model (e.g., see CMIP6 climate projections, 2021 and ACCESS-CM2, 2024) was used for the present analysis. This model has a 1.25° spatial resolution for atmospheric variables and a 0.5° resolution for ocean variables. Data for January-June 2024-2050 were obtained at monthly resolution for 2 m air temperature, SST, and pack ice concentration and thickness. Model output was obtained for the Shared Socioeconomic Pathway (SSP) 2-4.5 scenario, which assumes that global carbon emissions maintain approximately current levels before starting to decrease around 2050 but not reaching net-zero by 2100 (e.g., see Allen, et al., 2017). This scenario is currently considered the most likely pathway humanity will follow (e.g., see Pielke, Jr., et al., 2022).

Figure 14 shows the annual January-June mean projected air temperatures and SSTs for 2024-2050 at the Makkovik Bank IPS location. Figure 15 shows the mean annual January-June projected sea ice concentrations (a) and thicknesses (b) for the same period and location. Surprisingly, there is little overall projected trend in any of these variables with potentially a slight increase in air temperatures and SSTs accompanied by a slight decrease in ice concentration and thickness; however, strong interannual variability (and therefore unpredictability and uncertainty) in temperatures and ice conditions can be expected due to interannual internal variability in climate indices such as the NAO which have a strong impact on weather in the North Atlantic region.

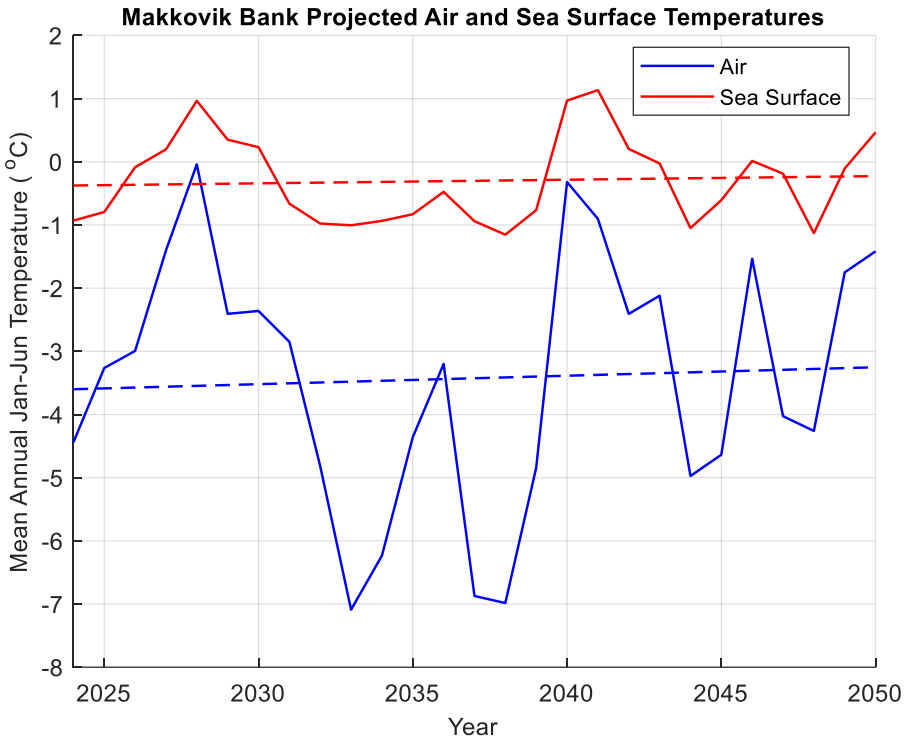

Figure 14. Makkovik Bank ice season projected mean air and sea surface temperatures, 2024-2050.

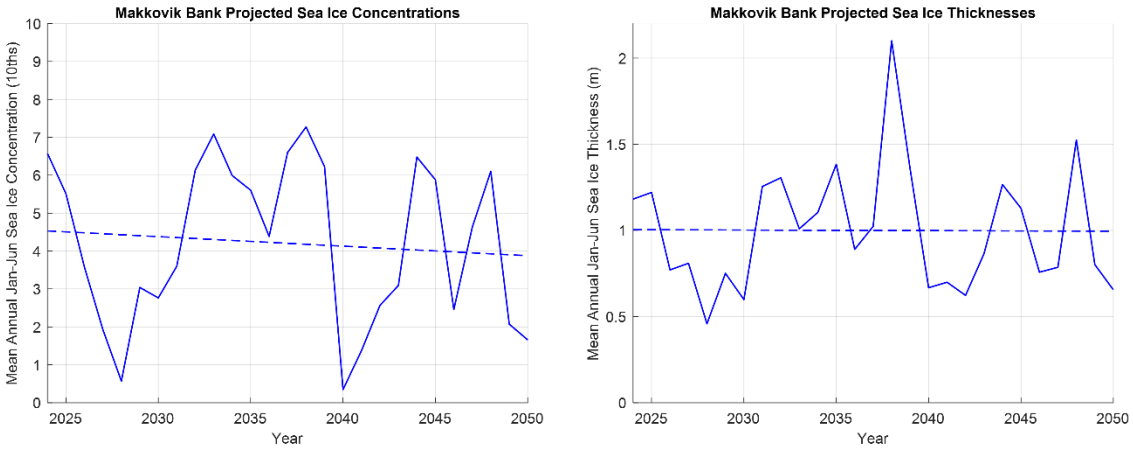

Figure 15. Makkovik Bank ice season projected mean sea ice concentrations (a) and thicknesses (b), 2024-2050.

Table 3 summarizes the slopes and R^2 values for the least-squares linear regression trend lines shown in previous figures. Given the limited dataset of only five ice seasons thus far, most of the trends are not yet strong or statistically significant. However, the increase in surface net energy flux stands out as potentially significant. We expect to be able to discern increasingly more statistically significant trends as more seasons of pack ice data are collected.

Table 3. Slopes and R^2 values for least-squares linear regression trends.

Variable	Slope	R^2	Figure
Pack Ice Season Length (days yr^{-1})	0.40	0.03	5b
Pack Ice Mean Thickness (m yr^{-1})	-0.04	0.16	6a
Pack Ice Thickness Standard Deviation (m yr^{-1})	-0.01	0.04	6a
Pack Ice Maximum Thickness (m yr^{-1})	-0.31	0.11	6b
Makkovik Bank Mean Surface Energy Flux ($Wm^{-2}yr^{-1}$)	1.60	0.75	11a
Makkovik Bank Mean Basal Energy Flux ($Wm^{-2}yr^{-1}$)	-10.34	0.33	12a
Projected Mean Air Temperature (°C yr^{-1})	0.01	0.00	14
Projected Mean SST (°C yr^{-1})	0.01	0.00	14
Projected Mean Ice Concentration (yr^{-1})	-0.03	0.01	15a
Projected Mean Ice Thickness (m yr^{-1})	0.00	0.00	15b

CONCLUSIONS

The results in this paper point toward a decreasing trend in pack ice mean and maximum thickness on the Makkovik Bank over 2003-2023, possibly linked to an increasing trend in regional January-June mean air temperatures and surface incident solar radiation and therefore increasing surface ice melt. However, these trends are based on an extremely limited dataset of only five ice seasons thus far. It will therefore be critical to continue such data collection efforts years into the future to continue monitoring the regional ice regime and building a statistically robust dataset to assess emergent trends. The analysis of regional environmental conditions and energy fluxes over the five ice seasons reveals a complicated picture, with a decrease in SSTs and basal ice energy fluxes contrasting with an increasing trend in air temperatures and surface net energy fluxes mainly due to increasing incident solar radiation. According to the simple surface energy flux model used in this paper, the increase in solar radiation over time is linked to a decrease in cloud cover. The analysis of future climate change on the Makkovik Bank, while limited in this paper, points to a potential future of decreasing ice concentrations and thicknesses with rising air and ocean surface temperatures, albeit with significant interannual variability, unpredictability, and therefore uncertainty in pack ice conditions and temperatures. The offshore Labrador region is subject to large interannual variations in temperatures due to the influence of the North Atlantic Oscillation (NAO, e.g., see Carroll, 2023), which could have a significant influence on interpreting trends with a limited duration of data.

The main goal of this paper was to introduce the renewed Makkovik Bank pack ice data collection campaign and highlight that this ongoing effort will build a critical dataset for monitoring trends in the regional ice regime over time, especially given that it builds on the existing pre-2010 dataset containing four seasons of ice draft data. Future work will focus on continued analysis of the dataset as it is built, and more robust trends can be assessed. Expanded analysis of climate model output from other models and carbon emissions scenarios will also be considered, as well as comparison of observed trends with those predicted from the climate models. Future work will also examine trends in pack ice drift velocities, floe sizes, and seasonal number of ice-free days, in addition to thickness.

The future results of this project will have implications for offshore structure and vessel design for energy development and shipping as a lessening of the severity of the ice regime could lead to significant cost savings in ice design. Interest in continued oil and gas and potentially new wind energy development offshore southeastern Newfoundland will be impacted as the pack ice that drifts into this region initially often drifts through the Makkovik Bank region.

ACKNOWLEDGEMENTS

We thank Fisheries and Oceans Canada (DFO) for providing the 2003-2009 IPS data from Makkovik Bank. We thank the Government of NL Department of Industry, Energy and Technology (IET) for providing funding for the redeployment of the instrumentation on Makkovik Bank in 2022. We thank Equinor for funding the data analysis for the 2022-2023 season. We thank Rodd Laing of the Nunatsiavut Government for in-kind support for this work, and Joey Angnatok for providing vessel access for deployment and recovery of the instrumentation.

REFERENCES

ACCESS-CM2, 2024. Australian Community Climate and Earth System Simulator (ACCESS). [Online] Available at: https://research.csiro.au/access/about/cm2/ [Accessed on December 11, 2024].

Allen, M. et al., 2017. Frequently asked questions. [Online] Available at: https://www.ipcc.ch/site/assets/uploads/sites/2/2018/12/SR15_FAQ_Low_Res.pdf [Accessed on December 11, 2024].

ASL Environmental Sciences Inc., 2024. *ASL Field Report Makkovik Bank IPS Study, September 2024*.

ASL Environmental Sciences Inc., 2009. *Data Processing and Analysis of Ice Keel Depths and Ice Velocities, Makkovik Bank, 2002-2009*.

Ballicater Consulting Ltd., 2012. *Ice Island and Iceberg Studies 2012*, Canadian Ice Service, Environment Canada, Report 12-01.

Bourke, R.H., & Paquette, R.G., 1989. Estimating the Thickness of Sea Ice. *Journal of Geophysical Research*, 94(C1), pp. 919-923.

Carroll, M., 2023. North Atlantic Oscillation contributes to ‘cold blob' in Atlantic Ocean. [Online] Available at: https://www.psu.edu/news/research/story/north-atlantic-oscillation-contributes-cold-blob-atlantic-ocean [Accessed on April 9, 2025].

CMIP6 climate projections, 2021. *Copernicus Climate Change Service (C3S) Climate Data Store (CDS)*, DOI: 10.24381/cds.c866074c [Online] Available at: https://cds.climate.copernicus.eu/datasets/projections-cmip6?tab=overview [Accessed on December 11, 2024].

Crawford, A.J., Mueller, D.R., Humphreys, E.R., Carrieres, T., & Tran., H., 2015. Surface ablation model evaluation on a drifting ice island in the Canadian Arctic. *Cold Regions Science and Technology*, 110, pp. 170-182.

Ebert, E.E., & Curry, J.A., 1993. An Intermediate One-Dimensional Thermodynamic Sea Ice Model for Investigating Ice-Atmosphere Interactions. *Journal of Geophysical Research*, 98(C6), pp. 10,085-10,109.

Han, G., Ma, Z., Long, Z., Perrie, W., & Chassé, J., 2019. Climate Change on Newfoundland and Labrador Shelves: Results from a Regional Downscaled Ocean and Sea-Ice Model Under an A1B Forcing Scenario 2011-2069. *Atmosphere-Ocean*, 57(1), pp. 3-17.

Hersbach, H., Bell, B., Berrisford, P., Biavati, G., Horányi, A., Muñoz Sabater, J., Nicolas, J., Peubey, C., Radu, R., Rozum, I., Schepers, D., Simmons, A., Soci, C., Dee, D., Thépaut, J-N., 2023. ERA5 hourly data on single levels from 1940 to present. *Copernicus Climate Change*

Service (C3S) Climate Data Store (CDS), DOI: 10.24381/cds.adbb2d47 [Online] Available at: https://cds.climate.copernicus.eu/datasets/reanalysis-era5-single-levels?tab=overview [Accessed on December 11, 2024].

King, T., & Turnbull, I.D., 2022. The Changing Iceberg Regime and Links to Past and Future Climate Change Offshore Newfoundland and Labrador. *Journal of Ocean Technology*, 17(3), pp. 54-76.

King, T., Turnbull, I., & Stuckey, P., 2023. SIIBED: An Updated Subsea Iceberg Risk Model for the Grand Banks. *Proceedings of the Offshore Technology Conference (OTC)*.

Marks, D., & Dozier, J., 1979. A clear-sky longwave radiation model for remote alpine areas. *Archiv für Meteorologie, Geophysik und Bioklimatologie, Serie B*, 27, pp. 159-187.

Murray, F.W., 1967. On the computation of saturation vapour pressure. Journal of Applied Meteorology, 6(1), pp. 203-204.

Oilco, 2022. Metocean Climate Study – Offshore Newfoundland and Labrador, STUDY MAIN REPORT, Volume 2: Regional Trends and Comparisons with Other Regions.

Pielke Jr., R., Burgess, M.G., & Ritchie, J., 2022. Plausible 2005-2050 emissions scenarios project between 2°C and 3°C of warming by 2100. *Environmental Research Letters*, 17, 024027.